energy&fuels

Review

pubs.acs.org/EF

Understanding Shale Gas: Recent Progress and Remaining Challenges

Alberto Striolo*,† and David R. Cole‡

†Department of Chemical Engineering, University College London, WC1E 7JE, London, United Kingdom

‡School of Earth Sciences, The Ohio State University, Columbus, Ohio 43210, United States

ABSTRACT: Because of a number of technological advancements, unconventional hydrocarbons, and in particular shale gas, have transformed the US economy. Much is being learned, as demonstrated by the reduced cost of extracting shale gas in the US over the past five years. However, a number of challenges still need to be addressed. Many of these challenges represent grand scientific and technological tasks, overcoming which will have a number of positive impacts, ranging from the reduction of the environmental footprint of shale gas production to improvements and leaps forward in diverse sectors, including chemical manufacturing and catalytic transformations. This review addresses recent advancements in computational and experimental approaches, which led to improved understanding of, in particular, structure and transport of fluids, including hydrocarbons, electrolytes, water, and CO_2 in heterogeneous subsurface rocks such as those typically found in shale formations. The narrative is concluded with a suggestion of a few research directions that, by synergistically combining computational and experimental advances, could allow us to overcome some of the hurdles that currently hinder the production of hydrocarbons from shale formations.

INTRODUCTION

Unconventional hydrocarbons attract attention because conventional resources are dwindling, and because several scientific and technological challenges need to be addressed to achieve high production with minimal environmental impact. Shale gas generated a renaissance in the whole US industrial sector, from the substitution of coal power plants,[1,2] to large investments in the chemical industry.[2] The rest of the world is watching, as shale formations are ubiquitous, even in regions not blessed by large conventional reserves. The naïve course of action was first to correlate a local shale formation with one US play, followed by transfering the successful US technologies to the shale play overseas. This strategy is defective (e.g., in Poland industry stopped investments due to less-than-spectacular productivity).[3] The community learned that unless complex physical phenomena occurring in the subsurface are understood, production of shale oil and gas requires expensive and unattractive trial-and-error processes. Although important technological advancements led to impressive production improvements,[4,5] some major limitations remain: (a) the well productivity decreases rapidly[6] and (b) a large amount of gas remains unproduced despite multiple fracturing stages[7] and the use of advanced hydraulic fracturing fluids.[8]

Below we summarize progress made to understand the molecular phenomena responsible for these observations This progress has been made possible by leveraging innovative approaches from various research communities, which led to better understanding of how confinement affects fluid properties, and to a more detailed characterization of heterogeneous porous materials. This review focuses on recent advances in these areas, with relevance to shale rocks, in the development of models for describing shale pores, in advancements on mesoscale simulations suitable for predicting fluid transport, and in atomistic simulations for fluid mixtures at interfaces.

Building on this, we argue that measuring the pore network at the nanoscale and quantifying the fluid behavior at the interface between kerogen and the surrounding matrix, especially for mixtures where one component dictates the behavior of the others, are crucial to understand the rate-limiting steps in shale gas production, and to leap forward the related technologies. Securing progress in these areas is expected to yield important positive implications not only for developing shale gas, but also in catalysis, fine chemicals, and controlled drug delivery. This review is focused particularly on the kerogen−clay interface, but it should be pointed out, for completeness, that organic-rich and nonclay dominated shale formations do exist as well.[9] Other important aspects related to unconventional oil and gas operations, including the possibility of inducing microseismic events, treatment of the produced fluids, prevention of fugitive emissions, identification of biogenic vs thermo-genic hydrocarbons, local impacts on traffic and competition for land usage, the risk of spills, and other environmental contaminations are not considered in this review.

RECENT ADVANCES

Confined Fluids Behavior. Several groups employed molecular simulations to investigate fluids in a variety of pores of relevance for shale (porous carbons representative of kerogen, clay pores, carbonates, alumino-silicate, and other porous materials).[10−14] For example, Mosher et al.[15] showed that excess methane adsorption in carbon-slit pores decreases as the pore width increases from 0.4 to 9 nm. Liu and Wilcox quantified the preferential adsorption of CO_2 vs methane in

Received: April 10, 2017
Revised: August 3, 2017
Published: August 27, 2017

DOI: 10.1021/acs.energyfuels.7b01023
Energy Fuels XXXX, XXX, XXX−XXX

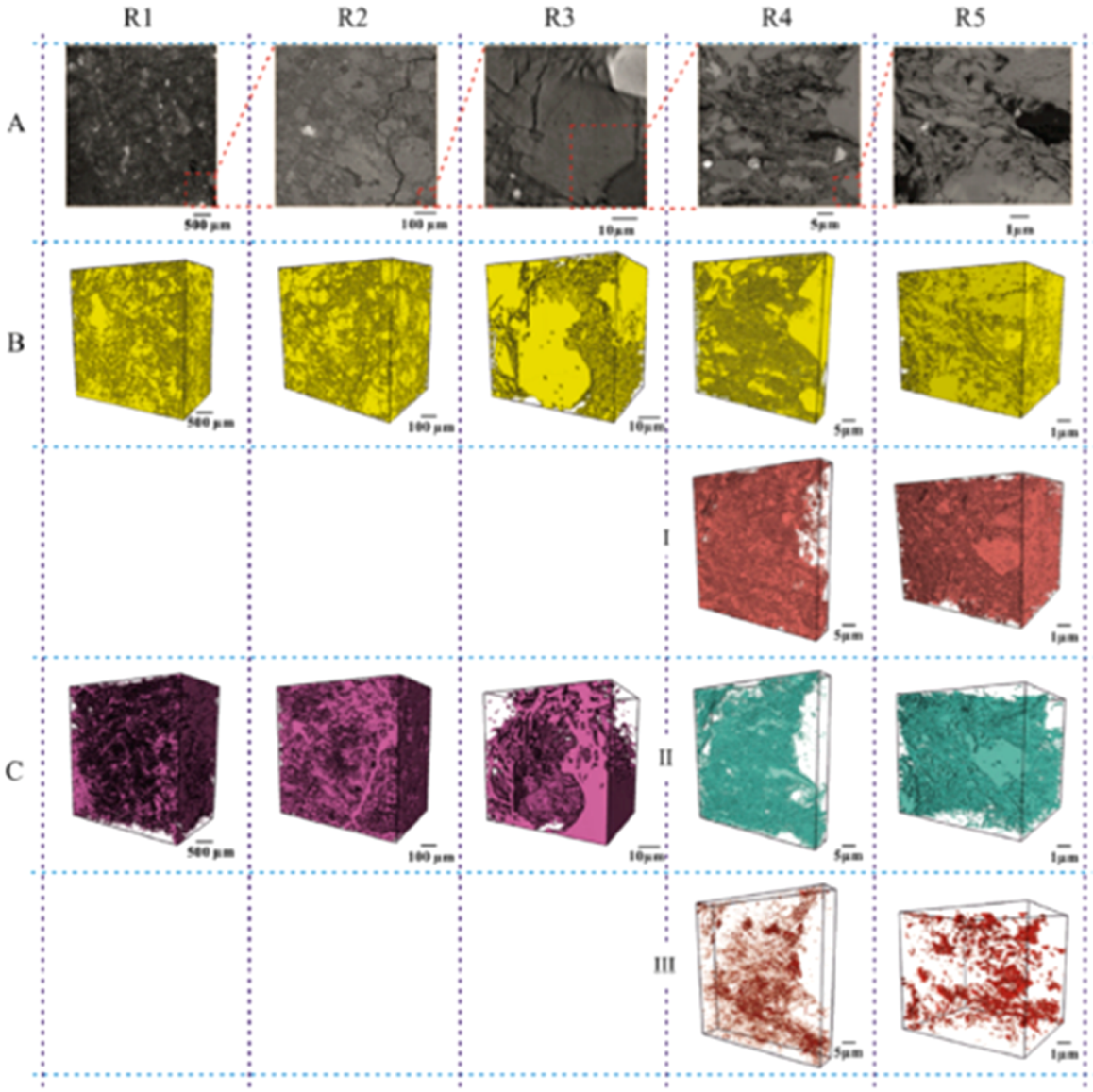

Figure 1. Ensemble of multiscale images of Bowland shale rock samples. Images in columns R1, R2, and R3 are X-ray CT scan reconstructions, while R4 and R5 are 3D-EM reconstructions. Row A reports 2D slices from the material, each enlarged from left to right. Row B highlights the nonclay minerals (e.g., dolomite, calcite, quartz, and pyrite), and their segmentation within the material. For R4 and R5 the authors managed to report the clay minerals (I), the organic matter (II), and the pores (III), which are shown in row C. For R1, R2, and R3 clay minerals, organic matter and pores are shown together (Reproduced with permission from ref 56. Copyright 2016 the authors of the original work).

oxygenated carbon-slit pores,[16] which is important because kerogen contains both carbon and oxygen and because CO_2 could be used to stimulate production. Oxygenated groups also favor water adsorption. Many simulated water adsorption in carbons,[17−24] including the work of Striolo et al.,[25,26] who considered a variety of carbon pores, sometimes with oxygenated groups,[27] and investigated the effect of temperature, achieving reasonable agreement against experiments.[28] By considering carbon slit pores of different widths, connected via apertures and defects, it was possible to recover experimental features, including smooth adsorption−desorption hysteresis loops.[29] These, and other studies, confirm that a detailed knowledge of the pore network is needed to understand confined fluids using molecular simulations.

Szczerba et al.[30] used molecular simulations to explain experimental spectroscopic observations for water in smectite clays. Szczerba and Kalinichev ranked various force fields based on their ability to appropriately reproduce experimental XRD measurements in organoclay systems.[31] Jeanmairet et al.[32] discussed how various simulation approaches can be implemented to describe, with atomistic precision, the hydration structure of clays.

Franco et al.[33] simulated methane and CO_2 in calcite pores and showed that strong solid−fluid interactions can yield anisotropic diffusion near the surface. Papavasileiou et al.[34] simulated water and one long hydrocarbon in titania pores. Water accumulated on the pore surface, where it formed hydrogen bonds with surface groups, while the hydrocarbon accumulated in the pore center. Phan et al.[35] showed that water from water−ethanol mixtures also accumulates on alumina surfaces, but also that when the pores are ∼1 nm in width, the water surface diffusion can be faster than that of ethanol, accumulated near the pore center. It has been shown that CO_2, adsorbed on a silica-based pore surface, lubricates the transport

DOI: 10.1021/acs.energyfuels.7b01023
Energy Fuels XXXX, XXX, XXX−XXX

of hydrocarbons within the pore.[36] Bui et al.[37] recently reported that methane, adsorbed at low concentration within hydrated pores, can show anisotropic diffusion depending on the chemistry of the confining material (i.e., anisotropic diffusion along the two directions parallel to the pore surface was reported for calcite, but not for muscovite, silica, or alumina pores).

Confinement is known to affect many thermodynamic properties of fluids.[38] Of particular importance to this review are the simulations of Luzar and Bratko,[39,40] who predicted the enhanced solubility of gases in confined fluids. Those initial predictions were later confirmed experimentally.[41,42] More recently, Gubbins and co-workers[43] studied the solubility of supercritical gases in liquids confined in narrow slit-shaped carbon pores. The solubility strongly depends on pore width and on packing densities and it decreases as temperature increases, but faster in confinement than in bulk systems. Although conducted for simple Lennard-Jones models, the results of Hu et al.[43] are consistent with those of Phan et al.,[44,45] who reported enhanced methane solubility in water confined in narrow slit-shaped pores. It remains to be completely understood how the structure of confined water can in some cases enhance and in some cases depress the solubility of guest gases. As an example of a study in which confinement reduces the solubility in water, we refer to Lisal and co-workers,[46] who used Monte Carlo simulations to quantify the solubility of NaCl in water confined in slit-shaped pores of width 0.7 to 2.8 nm carved out of pyrophyllite and Na-montmorillonite. The results show that the NaCl solubility decreases with pore size, and also revealed a significantly different behavior of the electrolytes depending on their preferential adsorption within the pore. In fact, Moucka et al.,[47] also using simulations, reported that salt uptake in aqueous pores is modulated by pore width. These results are probably related to both the structure of confined water and to the effect of confinement on the dielectric constant. Indeed, it is expected that confinement strongly affect the dielectric profile of water, depending on the confining material, pore width and shape, and also on the direction of interest (e.g., parallel vs perpendicular to the pore surface).[48−52]

This body of work demonstrates that depending on pore size, chemistry and composition, fluids behave differently under confinement compared to what we expect from bulk observations. While neutron scattering confirms some of these predictions,[53] one should question whether these molecular-level observations yield noticeable macroscopic effects. For example, how are the confinement effects on fluid solubility and diffusion determining natural gas transport across complex subsurface porous networks and, ultimately, the production of shale gas? *Identifying the connection between molecular features and macroscopic observables remains a grand scientific challenge.*

Characterization of Pore Networks. As discussed above, simulating confined fluids requires the definition of the solid substrate, if possible with atomic precision. Because shale samples are extremely diverse, this task is prohibitive. Based on a combination of experimental tools including small angle neutron scattering and backscattered electron microscopy, it has been found that 50% of the pores in shale samples can have size of less than 20 nm,[54] which makes the characterization harder. However, progress is tangible.[55] Ma et al.[56] used X-ray computed tomography and SEM to produce 3D images of shale samples. The resolution achieved spans 3 orders of magnitude, from 7 nm to ∼7.7 μm. The data showed a variety of pore scales and detected no visible connected porosity of size >20 nm. This clearly indicates the importance of small pores for understanding shale fluids. The data, reproduced in Figure 1, suggest that organic matter could provide connected pathways, although the resolution was not sufficient for detecting them. Other cutting-edge tools include FIB-SEM, used by Chen et al.[57] to obtain the 3D internal structure of kerogen. The analysis resolved kerogen, clay minerals, and pyrite, and individual pores were reconstructed with a 12 nm resolution (731 pores were identified within a kerogen specimen of size 3360 nm × 1440 nm × 1200 nm). The kerogen pores were roughly spherical, isolated from each other, and the surrounding rock, yielding ∼30% porosity.

Focused ion beam (FIB) SEM is finding a growing number of applications in the earth sciences particularly in the study of submicron pore network in shale.[58] This method uses serial sectioning and imaging in order to produce sets of sequential SEM images (generally several hundred) that permit a three-dimensional (3D) visualization of minerals, organics, and pores. From these 3D images, one can calculate porosity, pore-size distribution, kerogen volume percentage, and permeability.[59−63] Silin and Kneafsey discuss some of the issues encountered with FIB/SEM applications.[64] One of the major limitations of FIB/SEM is the extremely small size of the sample area. Therefore, when performing nanometer-scale interrogations of fine-grained, low porosity materials like shale, it is important to consider the scale of the observation in the context of the scale of interest. Volumes of 20 μm × 10 μm × 5 μm are typically imaged. Hence the sample may be 20 to nearly 30 orders of magnitude smaller than the lithologic unit it is meant to represent. A case in point is illustrated in images shown in Figure 2. This FIB/SEM sample comes from the Utica formation, Wood County, West Virginia, at a depth of 9502.7 feet.[65] In this deep part of the Appalachian Basin the Utica is roughly 300 feet thick; and the formation extends

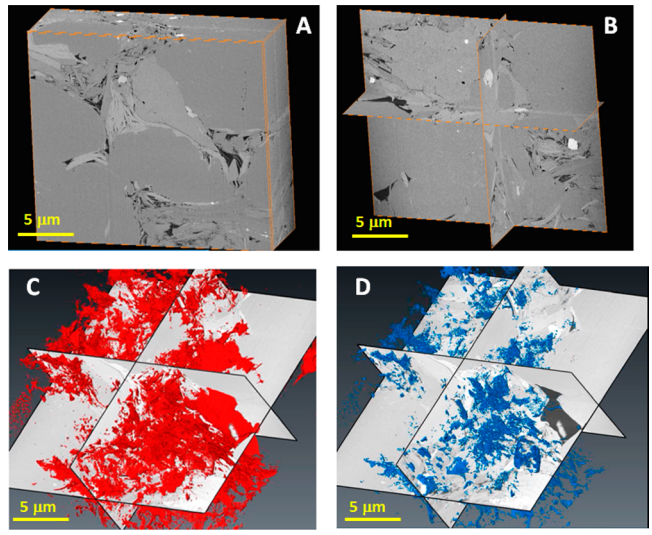

Figure 2. (A) Dual beam FIB/SEM reconstructed block volume of a deep Utica shale sample. (B) 3D "fence" image. (C) 3D reconstructed images of kerogen (red) distributions. (D) 3D reconstructed images of pores (blue) distributions. The 3D reconstructed volumes have dimensions of 20 μm × 17 μm × 6.5 μm. Panel A is reproduced with permission from ref 65. Copyright 2014 Mineralogical Society of America.

DOI: 10.1021/acs.energyfuels.7b01023
Energy Fuels XXXX, XXX, XXX−XXX

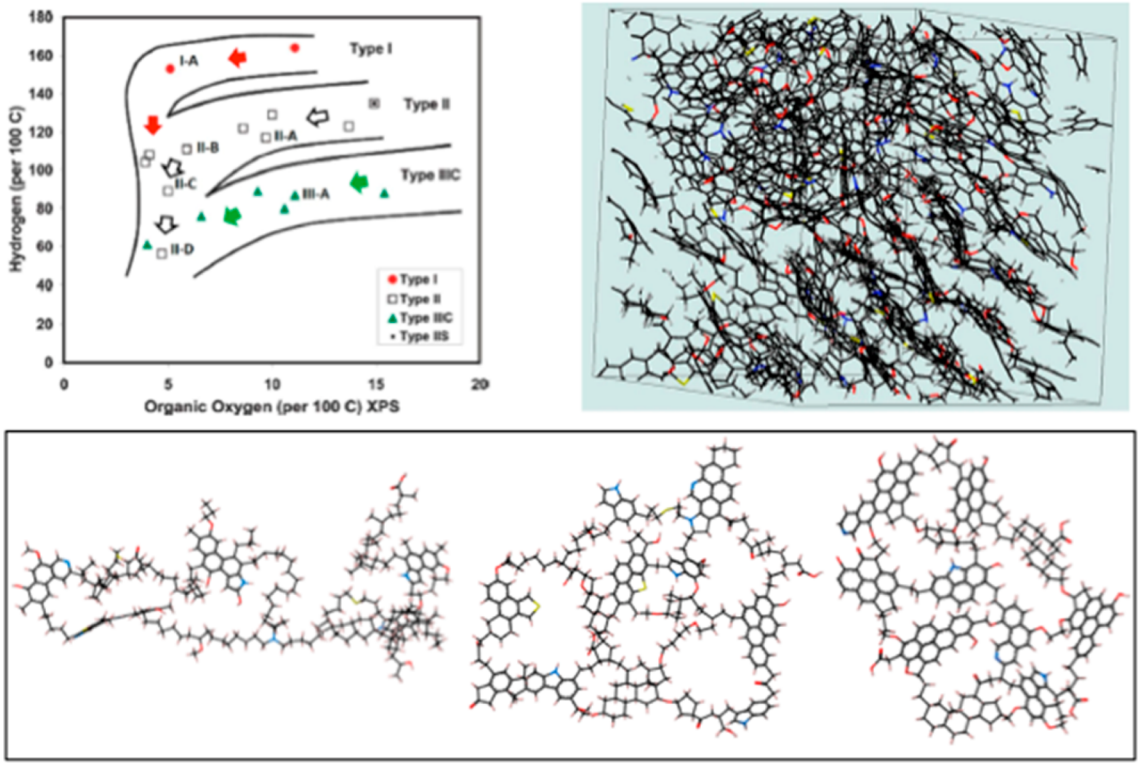

Figure 3. (top left) Van Krevelen diagram,[88] which indicates the three main types of kerogen, and their chemical composition, as a function of thermal maturity. (bottom) Three molecular units of kerogen developed by Ungerer et al.[87] From left to right, three models referred to as type I-A, type II-A, and type III-A, with chemical formulas $C_{251}H_{385}O_{13}N_7S_3$, $C_{252}H_{294}O_{24}N_6S_3$, and $C_{233}H_{204}O_{27}N_4$, respectively. (color code): C (black), H (gray), O (red), N (blue), S (yellow). (top right) Final configuration of a system containing 12 model type II-D units, whose chemical formula is $C_{175}H_{102}O_9N_4S_2$, simulated at 300 K and 1 bar. This snapshot provides a model for the kerogen inclusion in a shale rock (Adapted with permission from ref 87. Copyright 2015 American Chemical Society).

north, northwest, and northeast for several hundred kilometers. The pores (Figure 2C) within this sample occur primarily within the kerogen (Figure 2B) and exhibit a fair degree of connectivity, but the image is only ~20 μm across.

A second issue impacting pore assessment is that sampling bias must be taken into account. Most geologic materials exhibit some form of heterogeneity that may cross a variety of length scales. For example, in the case of shales they are usually anisotropic in the form of thin laminae and contain pores ranging in scale from tens of micrometers down to below 10 nm (e.g., see Figure 1). The porosity may vary within a given layer and between layers, as might permeability both of which are also typically anisotropic. Despite these and other limitations (e.g., rheologic integrity, sample preparation, sample deterioration during the experiment), nanoscale imaging via FIB/SEM has a number of advantages. As noted above, from the images one can obtain a fundamental understanding of the 3D nature of pore space, pore connectivity, and the location and distribution of mineral and organic phases. The images provide a foundation for conceptual model building that leads to quantification of permeability and fluid flow. Recently this approach has been used to estimate the accessible surface area in the Lower Tuscaloosa sandstone.[62] Mineral distributions mapped in 2D by SEM/EDX were coupled with dual-beam FIB/SEM and X-ray-based micro tomographs of select regions within the samples to quantify the connected pore network.

We point out that the visualization of pore networks is essential for interpreting additional experiments, e.g., adsorption isotherms, used to estimate the gas in place, and permeability. Heller and Zoback[66] recently measured the adsorption of methane and CO_2 on shale samples from the Barnett, Eagle Ford, Marcellus, and Montney plays. The measurements, performed at 40 °C and up to ~100 bar, showed that "CO_2 has ~2−3 times the adsorptive capacity of methane", suggesting that CO_2 could be used to stimulate shale formations, enhance methane recovery, and perhaps be permanently sequestered. The authors also suggested that "water adsorption plays an important role in regulating surface area availability for other molecules to adsorb". Based on the literature on activated carbons, this seems a distinct possibility. Brennan et al.,[67] e.g., already in 2002 reported that water adsorption in carbons can block access to methane, reducing adsorption capacity.

Although laboratory permeability measurements on shale samples are notoriously difficult because of the low signal-to-noise ratio, a number of data are appearing. Bhandari et al.[68] reported measurements for Barnett samples and provided a complete overview: permeability values in shale samples vary by several orders of magnitude. The data depend on the applied effective stress, on the orientation of bedding relative to the flow direction, and on many other factors, including the presence of water. Bhandari et al.[68] report permeability as low as 2 nanodarcy, and anisotropy of ~40 (ratio between permeability measured in two directions) for their samples, which had 4% total organic content and were composed predominantly of quartz, calcite, and clay. Data measured for a variety of samples show permeability in the range 0.1 to 1000 nanodarcy.[69−71] Permeability decreases by up to several orders

DOI: 10.1021/acs.energyfuels.7b01023
Energy Fuels XXXX, XXX, XXX−XXX

of magnitude upon increasing the effective stress by 20−30 MPa.[72−74] Reported permeability anisotropy ranges from as little as ∼5, to 10,000 or more.[75,76] These limited data confirm what has become the mantra in shale rocks characterization: every shale rock is uniquely different. What needs to be identified, completely understood, and possibly quantified are the unique descriptors that could lead to the prediction of fluid behavior within a unique rock formation. In other words, what measurements need to be done to design and optimize the stimulation strategy for a given subsurface formation?

Models for Shale Pores. As discussed above, shale includes diverse rock types, with kerogen dispersed in matrixes, sometimes crystalline. Molecular models for crystalline rocks are available in the literature. CLAY-FF, e.g., was derived for describing clays,[77] yielding excellent results for clay−water interfaces.[78−83] The model is being improved to include edges,[84,85] which is needed to investigate the entry of fluids in pores, and polarizability.[86] Calcite, quartz, and other relevant minerals can be described using their crystalline structure.[37]

Models for kerogen are more difficult to derive. Many build on the models developed by Ungerer et al.,[87] whose kerogen units reproduce experimental elemental composition and functional groups.[88] Atomistic and first-principles simulations using these models (Figure 3) yield density and heat capacity in good agreement with experiments. Other models can be derived, but they should identify narrow pores and a density of oxygenated groups consistent with the Van Krevelen diagram.[88] Orendt et al.,[89] e.g., proposed both a general approach and a 3D model for the Siskin Green River oil shale kerogen. Alternative approaches to generate nanoporous models for carbons include hybrid reverse Monte Carlo and quenched molecular dynamics approaches, sometimes implementing reactive force fields.[90−92] Recently, for example, Economou and his group developed and tested a family of kerogen models.[93] They quantified the porosity of their kerogen models, which was controlled by depositing "dummy" Lennard-Jones spheres within the system as it was being prepared. These dummy spheres were then removed once the material was prepared, and then, the pore space was quantified using both conventional and newly developed computational approaches. The approach allowed them to prepare models with percolated porosity, which could be useful for better understanding the behavior of confined fluids using molecular simulations. They tested these models against the predicted adsorption of pure methane as well as that of a mixture containing methane, ethane, and propane, and also in terms of density of the kerogen structure. Economou and co-workers were able to identify systems that reproduce some of the porosity features that are expected to be present in kerogen samples.

Mesoscale Simulations. Ultimately, studying fluids in pores and nanopores should lead to large-scale simulations that estimate the productivity of a formation depending on wells geometry, fracturing stages, stimulation strategy, etc. Ross et al.[94] provided an example of such an application to determine whether CO_2 could be deployed to both enhance methane recovery and achieve long-term storage in the Powder River basin. The critical question is: *how can we assess whether molecular-scale details such as those discussed above have practical implications*? Answering this question is a current grand challenge.[95]

To tackle this grand challenge, one could implement multiscale approaches,[96] using the atomistic/molecular-level results as input. Chen et al., e.g., used Lattice Boltzmann computational fluid dynamics[98] to study the permeability through the shale rock sample characterized using FIB-SEM. While the results were encouraging, the authors conclude that "*more work is needed to better describe the adsorption and dissolution of gas molecules in intrakerogen pores and upscale them to the larger scale*". Other groups also used Lattice Boltzmann.[97] An alternative approach uses analytical theories, building on the effective medium theory, EMT, as proposed by Bonilla et al.[99] This approach is successful when the pore network is truly isotropic and disordered for all pore types.[100−103] However, when applied to hierarchical porous materials in which some of the pores are not homogeneously distributed, the EMT replicates experimental data with unreasonable values for its parameters, including the network connectivity.[104] *Perhaps one intermediate step is required to up-scale molecular insights to fluid dynamics and/or theoretical approaches.*

One methodology that could provide this intermediate step is kinetic Monte Carlo, KMC,[105−111] widely used in catalysis.[106] To study transport in porous networks, one KMC approach could identify the probability with which molecules occupy sites/regions within the material, the differences in free energy between the preferential adsorption sites/regions, and the energy barriers between consecutive adsorption sites.[112] Alternatively, one could subdivide the pore network in voxels (volume elements), describe the probability of observing molecules within each voxel, the ease of transport from one voxel to another, eventual barriers encountered in so doing, and changes in these characteristics due to molecule−molecule interactions.[113] The latter approach allows one to describe various parts of a pore, including regions filled with water through which molecules of interest adsorb and diffuse, etc.

Fluid Mixtures at Interfaces. The KMC approach could describe the different interfaces encountered by the fluid as it is transported from kerogen to the larger fractures. It is then crucial to better understand how the fluid properties change along this path.

Our survey must start inside kerogen, where important insights can be borrowed from the zeolite literature,[114] which provides diffusion coefficients as a function of cage size and coverage, and activation energies.[115,116] For mixtures in zeolites, it has been observed that the diffusion of the more mobile component can be blocked by another, less mobile compound (i.e., benzene can block methane).[117,118] These insights might have relevance for shale rocks, because the size of the pores in kerogen can be comparable to those found in zeolites. One clear difference is that pores are crystalline in zeolites and disordered in kerogen (see Figure 3). It is widely anticipated that as the pore size decreases, pore surface effects become dominant, and surface diffusion can become more important than "pore" diffusion (pore diffusion refers here to that of fluids not in contact with the surface), and preferential adsorption sites could affect both structure and dynamics of confined fluids. Indeed, Falk et al.[119] simulated hydrocarbons in a kerogen model considered realistic because it is disordered and because its pores have nanometer dimensions. The results unequivocally show that continuum hydrodynamics breaks down at the conditions considered (hence classic approaches such as Darcy's law fail), although the permeability could be described knowing each hydrocarbon's length and density. Building on these observations, Obliger et al.[120] simulated hydrocarbon mixtures in kerogen. The results suggest that "owing to strong adsorption effects, velocity cross correlations between the mixture components and between molecules of

DOI: 10.1021/acs.energyfuels.7b01023
Energy Fuels XXXX, XXX, XXX−XXX

the same species are [...] negligible". This suggests that the behavior of one fluid does not affect the behavior of another, which seems at odds with observations in zeolites and could be a consequence of the fact that Obliger et al. only considered simple alkanes.

The next family of simulation studies of interest to this overview concerns the *mechanisms by which methane escapes kerogen*: Ho et al.[121] found that (a) 30−47% of the gas recovery is due to the fast release of pressurized free gas, present within the nanopores; (b) this is followed by the slow desorption of adsorbed gas, which diffuses out of the pores; (c) 3−35% of the gas remains trapped in isolated nanopores, and therefore nonrecoverable. Lee et al.[122] studied the escape of methane from a kerogen model when water provides a barrier (see Figure 4). The results showed that methane desorption is an activated process, in which the activation energy (barrier) increases as the pressure drop across the material decreases. These interesting results depend on the nature of the interface between kerogen and the surrounding clay-rich rock, as well as on the fluid mixture present at that interface. Lee et al. suggested that "replacing water by CO_2 or propane eliminates the barriers, therefore raising hopes for clean/efficient recovery", and showed that the barrier strongly depends on the fraction of the solid surface that is hydrophilic, because of the work that needs to be done to remove interfacial water. These observations demonstrate that atomistic models can help identify strategies for optimizing the recovery of hydrocarbons. For example, based on the work of Heller and Zoback:[66] could CO_2 stimulation extract the ∼35% of natural gas trapped in kerogen? Could methane be permanently trapped in kerogen by using the wrong fluids?

The next stage investigates hydrocarbon transport through the surrounding clay-rich rock. Ho and Striolo[123] simulated water and methane in muscovite, a proxy for nonswelling clays. Depending on the amount of water present, and on the pressure applied perpendicularly to the pore surfaces, water could form a capillary bridge across the pore. This capillary bridge can block methane transport when it is oriented perpendicularly to flow. When the pressure drop in the direction parallel to the pore surface is large, the bridge becomes parallel to flow, restoring fast transport. Because the water bridges depend on water−methane interfacial tension, adding compounds such as CO_2 or surfactants could favor the dissolution of such bridges, thus enhancing hydrocarbon transport, perhaps explaining recent field observations.[8]

■ POSSIBLE WAYS FORWARD

While the research summarized above requires further progress to secure large positive impacts toward the sustainable production of shale gas, we argue that three main areas require immediate attention: (1) determine experimentally the structure of the interface between kerogen and the surrounding clay-rich matrix in representative shale samples, enhancing the resolution and possibly visualizing fluid transport through the pore network to interpret macroscopic permeability measurements and to provide validation for computational efforts; (2) continue the simulations of confined fluids, but focus on complex mixtures at interfaces between different porous media; and (3) develop mesoscale computational approaches that lead to sensible integration of the experimental characterization results with new and existing molecular simulation data to predict fluid transport in complex pore networks, therefore identifying the rate-limiting steps in shale gas production.

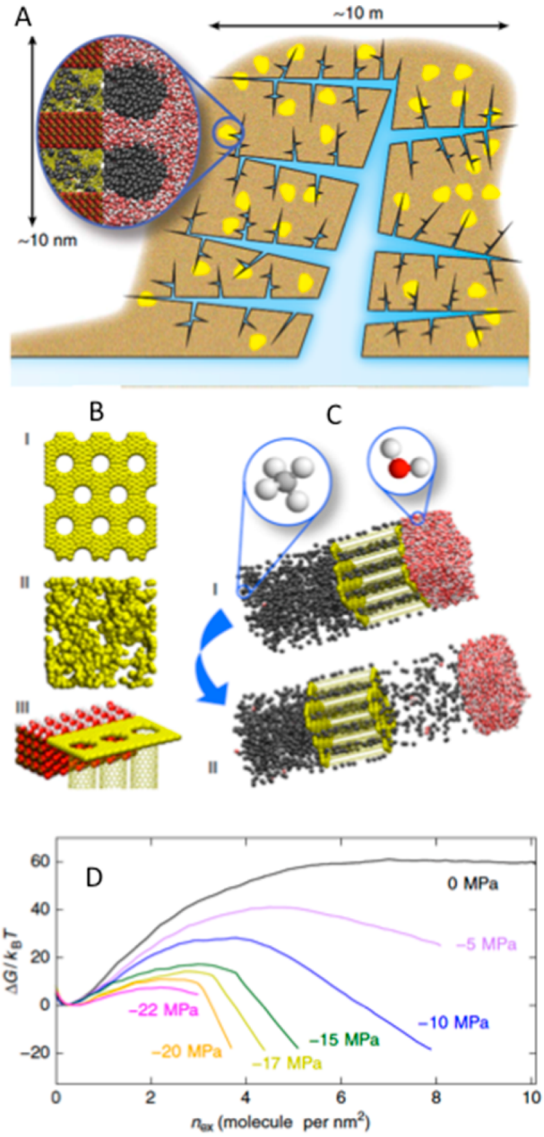

Figure 4. (A) Schematic of the system considered by Lee et al.[122] The hydraulically fractured shale formation brings water into contact with kerogen, within which methane is stored. (B) Three models considered methane desorption: (I) an array of carbon nanotubes, (II) a disordered carbon material, and (III) an array of carbon nanotubes surrounded by hydrophilic rock. (C) Process during which methane (gray spheres) moves from left to right and displaces the water film (red and white spheres). The "adhesion" of water to the solid substrate is responsible for the large energy barrier, quantified in panel D as a function of the applied pressure. When the pressure is high, the barrier is relatively small and methane can desorb, but when the pressure is low, the barrier is so large that methane may not be able to desorb from kerogen (Adapted with permission from ref 122. Copyright 2016 Nature Publishing Group).

Direct Imaging the Kerogen−Clay Interface. Important properties of shale samples depend on their 3D pore network at the atomic-, nano-, and mesoscales. As demonstrated in Figure 1, much progress has been made in characterizing shale rocks. Ellis and Peters,[124] e.g., combined X-ray computed tomography with scanning electron microscopy and X-ray spectroscopy to monitor changes in permeability due to the evolution of reactive fractures. However, *the resolution is still not sufficient to identify individual nanometer-sized pores.* Further, *the interface between kerogen inclusions and the surrounding matrix has*

DOI: 10.1021/acs.energyfuels.7b01023
Energy Fuels XXXX, XXX, XXX−XXX

remained elusive because of the different contrast between the two materials. The X-ray tomography data shown in Figure 1 cannot identify pore networks below 20 nm, while the FIB-SEM data from Chen et al.[57] were obtained at the resolution of 12 nm. The pores in kerogen (see Figure 3) are of the order of 1 nm in size. This resolution can be achieved using transmission electron microscopy (TEM). TEM instruments capable of imaging materials with atomic resolution are now ubiquitous, but they only produce 2D projection images, averaging the structure along the viewing direction. To retrieve information regarding features and the 3D structure along the viewing direction, it is possible to use many 2D projections acquired at different viewing angles—i.e., electron tomography.[125] This requires a TEM capable of rotating a sample to different viewing directions while keeping it stable. Electron tomography then reconstructs the 3D morphology by aligning all projection images and combining them digitally to produce a faithful representation of the original object density distribution. The resulting reconstruction consists of 3D distribution of the electron scattering power of the sample materials. TEM and scanning TEM (STEM) images provide monotonic projections of density for specimens under certain imaging conditions and are most often used to reconstruct 3D density.[126] Typically, an electron tomography experiment requires that an image be taken every 1−2 degrees over a range of ±70 degrees of tilt limited by the physical limitations of the TEM sample chamber, holder, and specimen geometry. This can be done over micrometer-sized fields of view with nanometer scale resolution for samples up to about 300 nm in thickness, yielding a quantitative measurement of the 3D density distribution within the sample.

Electron tomography has been applied to porous materials such as calcite,[127] bone,[128] organosilicates,[129] silicon dioxide,[130] and concrete.[131] It appears an important step forward to attempt to integrate X-ray tomography with electron tomography. The X-ray tomography can provide information on the pore network at relatively large scales, while the electron tomography could provide pore-level details. Of course, significant hurdles need to be overcome, including the possibility that both X-rays and electron beams damage the samples and that the interface between kerogen and clay (or other matrix materials) could show different contrast, and therefore could be difficult to visualize. As an example of this possible development, in Figure 5 we report 3D electron tomography data of a cement-based system, in which pores of approximately nanometer size spaced ∼5−8 nm apart are visualized.[131] These pore sizes are comparable to what we expect to observe in shale samples. It appears that the challenges already addressed for materials other than shale samples are similar to those faced by the desire to further characterize rock samples. For completeness, it should be mentioned that Helium ion microscopy has been used to observe ore features of the order of ∼1 nm in size. King et al.[132] reported images of the organic porosity from shale samples that could be helpful in validating the pore models discussed above

Simulating Fluid Mixtures at Interfaces. Additional molecular simulations should be conducted for systems that reproduce the experimentally determined features of the kerogen−clay interface, to achieve results that are directly applicable to quantify hydrocarbon desorption from shale formations and to complement the large body of literature available regarding the simulation of fluids confined in narrow pores (see the brief discussion above). The first step in these

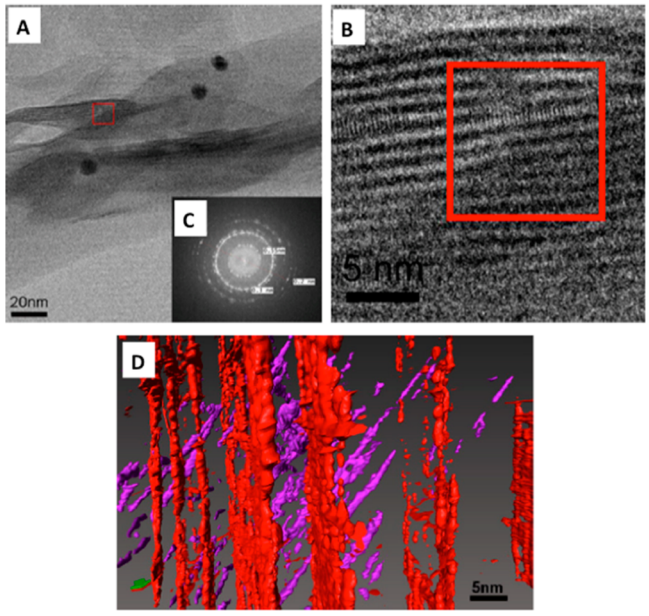

Figure 5. Experimental characterization data obtained using TEM for a cement-based paste. The paste was calcium silicate hydrate, and the sample was taken from the center of the paste. The high-resolution cryo-TEM (panel A) shows that the material is primarily amorphous, although some crystalline regions are observed. High-resolution details obtained from the crystalline region (panel B) illustrate the fine lattice fringes. The crystalline nature of this region is confirmed by selected area diffraction data (panel C). Using Xplore3D tomography software it was possible to reconstruct the 3D networks of the pores present in this material (panel D). Note that the pores are of size ∼1.7−2.4 nm and are separated by ∼5−8 nm. Reproduced with permission from ref 131. Copyright 2015 John Wiley and Sons.

studies would be the reconstruction of the confining material, based on experimental data. Two alternative approaches are possible for this: (a) idealization of system features toward reproducing some properties common to many shale plays or (b) use experimental details for deriving models as accurate as possible. In the context of shale gas, the former approach might yield results too general to be useful, while the latter could yield results so spatially restrictive as to not be representative even of a single formation. Keeping these limitations in mind, one should attempt to identify those features that are peculiar to the samples for which data are available, yet characteristic enough to yield generalizable observations. While the results will be strictly applicable to the model developed, it is possible that the approach will be generalizable, via the identification of appropriate descriptors and the implementation of appropriate coarse-grained approaches.

Using standard equilibrium and nonequilibrium simulation approaches one could select simulation systems to address fundamental questions such as How do fluids partition and adsorb when CO_2 or water are present at the kerogen−clay interface? How does the transport change when branched alkanes are present together with methane and propane within kerogen? Under what circumstances does the transport of the slowest compound dominate that of the other compounds at a kerogen−clay interface?

Multiscale Analysis of Fluid Transport. To attempt to quantify the mesoscale effects of the molecular-level details provided by the molecular simulations, one could implement a kinetic Monte Carlo model, KMC. Although several approaches

DOI: 10.1021/acs.energyfuels.7b01023
Energy Fuels XXXX, XXX, XXX−XXX

are possible, a voxel-based KMC model seems attractive. This approach requires a lattice model on which to run the simulations. The development of the lattice model requires experimental visualization of the sample of interest, as well as detailed information regarding the fluid properties in various pores. These could be obtained from characterization experiments. Using the KMC method one could then quantify how microscopic details (e.g., the presence of a water film at the interface between kerogen and clay, the presence of natural microfractures connecting several kerogen inclusions in a clay matrix,[133,134] fluid mixtures composed by large compounds that block the transport of small compounds) result in mesoscale observables such as the permeability of a rock fragment and its fracture network. Moreover, the characterization and the location of mesoscale interfaces such as kerogen/matrix, coarse grain/matrix, cluster of grains/matrix and interfaces between laminae are important to consider, in order to understand and predict fluid and fracture behaviors in such multiscale systems.[135,136] This information can be included in macroscopic simulators such as the one presented by Ross et al.,[94] or commercial ones.[137,138] One possible realization of a voxel-based KMC algorithm has been recently proposed by Apostolopoulou et al.[113] This approach has been validated in 1D and 2D against analytical descriptions of diffusion in homogeneous media, has reproduced molecular dynamics simulations for fluxes of various gases through nanopores filled with water,[45] reproduced expected trends for the fluid fluxes along 1D pores as a function of the pore length, and has been used to study gas transport in 1D models of pore networks. This model should now be extended to 3D pore networks and implemented to address critical questions that could help identify the rate-limiting steps in shale gas production.

CONCLUSIONS

Producing shale gas remains a challenge, both technological and scientific. However, much has been achieved in the past few years regarding improvements in both the characterization of subsurface formations and our understanding of fluids migration within them. Further progress seems achievable when state of the art approaches from diverse disciplines are synergistically combined. The importance of shale gas to both macro-scale economies and environmental concerns justifies significant investments on this topic even in a period when the oil price is far from its all-time highs. Some possible research directions are suggested in this review, which reflect the authors' opinions. These possible research adventures include: further simulations at the molecular level for realistic systems of technological importance, combined applications of advanced experimental characterization tools, including electron and X-ray tomography, and novel approaches to propagate microscale observations such as those attainable with molecular simulations toward predicting meso- and macroscopic observables. While the discussion is here focused on shale gas production, it is expected that the methods, once derived and optimized, could be applicable to a variety of sectors, ranging from construction to catalysis.

AUTHOR INFORMATION

Corresponding Author

*E-mail: a.striolo@ucl.ac.uk.

ORCID

Alberto Striolo: 0000-0001-6542-8065

Notes

The authors declare no competing financial interest.

ACKNOWLEDGMENTS

A.S. is grateful to a number of collaborators, in particular Dr. Ercius and Dr. Ashby at the Molecular Foundry, LBNL, and to all members of the consortium ShaleXenvironmenT (https://shalexenvironment.org) for continuous discussions on subjects relevant to the fundamental key questions that render shale gas such an interesting topic from both a fundamental and applied points of view. Mr. Tai Bui is particularly thanked for his help with formatting the manuscript. Financial support for this work was provided, in part, by the Sloan Foundation, via the Deep Carbon Observatory, the Marie Curie Career Initiation Grant No. 2013-CIG-631435, and the Department of Energy, Office of Basic Energy Sciences, Geosciences program under grant DE-SC0006878. This research received funding from the European Union's Horizon 2020 research and innovation program under grant agreement No. 640979.

REFERENCES

(1) Emanoel Siqueira Santos, V. E. S.; Rego, E. E.; Santos, E. M.; Ribeiro, C. O. Shale Gas and the Replacement of Coal-Fired Power Plants. *IEEE Lat Am. T* **2016**, *14* (8), 3721−3730.

(2) Liss, W. Demand Outlook: A Golden Age of Natural Gas. *Chem. Eng. Prog.* **2012**, *108* (8), 35−40.

(3) Shale gas exploration status in Poland as of March 2016. http://infolupki.pgi.gov.pl/en/exploration-status/news/shale-gas-exploration-status-poland-march-2016 (accessed March 16th, 2017).

(4) Workshop organized by the IEA Gas and Oil Technology Collaborative Programme, Global Dialogue: Unconventional Resource Development Enhanced Recovery and Environmental Stewardship, Austin, TX, October 12−13, 2016. http://www.gotcp.net/october-12-13-austin-tx (accessed March 16th, 2017).

(5) Krauss, C. Texas Oil Fields Rebound From Price Lull, but Jobs Are Left Behind. https://www.nytimes.com/2017/02/19/business/energy-environment/oil-jobs-technology.html.

(6) King, G. E. Hydraulic Fracturing 101: What Every Representative, Environmentalist, Regulator, Reporter, Investor, University Researcher, Neighbor and Engineer Should Know About Estimating Frac Risk and Improving Frac Performance in Unconventional Gas and Oil Wells. *SPE Hydraulic Fracturing Technology Conference* **2012**, DOI: 10.2118/152596-MS.

(7) Arogundade, O.; Sohrabi, M. A Review of Recent Developments and Challenges in Shale Gas Recovery. In *the SPE Saudi Arabia Section Technical Symposium and Exhibition*; Society of Petroleum Engineers: Al-Khobar, Saudi Arabia, 2012.

(8) He, K.; Xu, L.; Gao, Y. F.; Yin, X. L.; Neeves, K. B. Evaluation of surfactant performance in fracturing fluids for enhanced well productivity in unconventional reservoirs using Rock-on-a-Chip approach. *J. Pet. Sci. Eng.* **2015**, *135*, 531−541.

(9) Hart, B. S.; Macquaker, J. H. S.; Taylor, K. G. Mudstone ("shale") depositional and diagenetic processes: Implications for seismic analyses of source-rock reservoirs. *Interpretation-J. Sub* **2013**, *1* (1), B7−B26.

(10) Gubbins, K. E.; Long, Y.; Sliwinska-Bartkowiak, M. Thermodynamics of confined nano-phases. *J. Chem. Thermodyn.* **2014**, *74*, 169−183.

(11) Striolo, A.; Michaelides, A.; Joly, L. The Carbon-Water Interface: Modeling Challenges and Opportunities for the Water-Energy Nexus. *Annu. Rev. Chem. Biomol. Eng.* **2016**, *7*, 533.

(12) Wilcox, J.; Haghpanah, R.; Rupp, E. C.; He, J. J.; Lee, K. Advancing Adsorption and Membrane Separation Processes for the Gigaton Carbon Capture Challenge. *Annu. Rev. Chem. Biomol. Eng.* **2014**, *5*, 479.

DOI: 10.1021/acs.energyfuels.7b01023
Energy Fuels XXXX, XXX, XXX−XXX

(13) Gubbins, K. E.; Liu, Y. C.; Moore, J. D.; Palmer, J. C. The role of molecular modeling in confined systems: impact and prospects. *Phys. Chem. Chem. Phys.* **2011**, *13* (1), 58−85.
(14) Striolo, A. Interfacial water studies and their relevance for the energy sector. *Mol. Phys.* **2016**, *114* (18), 2615−2626.
(15) Mosher, K.; He, J. J.; Liu, Y. Y.; Rupp, E.; Wilcox, J. Molecular simulation of methane adsorption in micro- and mesoporous carbons with applications to coal and gas shale systems. *Int. J. Coal Geol.* **2013**, *109*, 36−44.
(16) Liu, Y. Y.; Wilcox, J. Molecular Simulation Studies of CO2 Adsorption by Carbon Model Compounds for Carbon Capture and Sequestration Applications. *Environ. Sci. Technol.* **2013**, *47* (1), 95−101.
(17) Liu, J. C.; Monson, P. A. Does water condense in carbon pores? *Langmuir* **2005**, *21* (22), 10219−10225.
(18) Barton, S. S.; Evans, M. J. B.; Macdonald, J. A. F. The Adsorption of Water-Vapor by Porous Carbon. *Carbon* **1991**, *29* (8), 1099−1105.
(19) Brovchenko, I.; Geiger, A.; Oleinikova, A. Water in nanopores. I. Coexistence curves from gibbs ensemble monte carlo simulations. *J. Chem. Phys.* **2004**, *120* (4), 1958−1972.
(20) Jorge, M.; Seaton, N. A. Predicting adsorption of water/organic mixtures using molecular simulation. *AIChE J.* **2003**, *49* (8), 2059−2070.
(21) Kaneko, K.; Hanzawa, Y.; Iiyama, T.; Kanda, T.; Suzuki, T. Cluster-mediated water adsorption on carbon nanopores. *Adsorption* **1999**, *5* (1), 7−13.
(22) McCallum, C. L.; Bandosz, T. J.; McGrother, S. C.; Muller, E. A.; Gubbins, K. E. A molecular model for adsorption of water on activated carbon: Comparison of simulation and experiment. *Langmuir* **1999**, *15* (2), 533−544.
(23) Muller, E. A.; Rull, L. F.; Vega, L. F.; Gubbins, K. E. Adsorption of water on activated carbons: A molecular simulation study. *J. Phys. Chem.* **1996**, *100* (4), 1189−1196.
(24) Slasli, A. M.; Jorge, M.; Stoeckli, F.; Seaton, N. A. Water adsorption by activated carbons in relation to their microporous structure. *Carbon* **2003**, *41* (3), 479−486.
(25) Striolo, A.; Chialvo, A. A.; Cummings, P. T.; Gubbins, K. E. Water adsorption in carbon-slit nanopores. *Langmuir* **2003**, *19* (20), 8583−8591.
(26) Striolo, A.; Chialvo, A. A.; Gubbins, K. E.; Cummings, P. T. Water in carbon nanotubes: Adsorption isotherms and thermodynamic properties from molecular simulation. *J. Chem. Phys.* **2005**, *122* (23), 234712.
(27) Striolo, A.; Chialvo, A. A.; Cummings, P. T.; Gubbins, K. E. Simulated water adsorption in chemically heterogeneous carbon nanotubes. *J. Chem. Phys.* **2006**, *124* (7), 074710.
(28) Striolo, A.; Gubbins, K. E.; Gruszkiewicz, M. S.; Cole, D. R.; Simonson, J. M.; Chialvo, A. A.; et al. Effect of temperature on the adsorption of water in porous carbons. *Langmuir* **2005**, *21* (21), 9457−9467.
(29) Striolo, A.; Gubbins, K. E.; Chialvo, A. A.; Cummings, P. T. The effect of pore connectivity on water adsorption isotherms in non-activated graphitic nanopores. *Adsorption* **2005**, *11*, 337−341.
(30) Szczerba, M.; Kuligiewicz, A.; Derkowski, A.; Gionis, V.; Chryssikos, G. D.; Kalinichev, A. G. Structure and Dynamics of Water-Smectite Interfaces: Hydrogen Bonding and the Origin of the Sharp O-D-W/O-H-W Infrared Band from Molecular Simulations. *Clays Clay Miner.* **2016**, *64* (4), 452−471.
(31) Szczerba, M.; Kalinichev, A. G. Intercalation of Ethylene Glycol in Smectites: Several Molecular Simulation Models Verified by X-Ray Diffraction Data. *Clays Clay Miner.* **2016**, *64* (4), 488−502.
(32) Jeanmairet, G.; Marry, V.; Levesque, M.; Rotenberg, B.; Borgis, D. Hydration of clays at the molecular scale: the promising perspective of classical density functional theory. *Mol. Phys.* **2014**, *112* (9−10), 1320−1329.
(33) Franco, L. F. M.; Castier, M.; Economou, I. G. Anisotropic parallel self-diffusion coefficients near the calcite surface: A molecular dynamics study. *J. Chem. Phys.* **2016**, *145* (8), 084702.
(34) Papavasileiou, K. D.; Makrodimitri, Z. A.; Peristeras, L. D.; Chen, J. Q.; van der Laan, G. P.; Rudra, I.; Kalantar, A.; Economou, I. G. Molecular Simulation of n-Octacosane-Water Mixture in Titania Nanopores at Elevated Temperature and Pressure. *J. Phys. Chem. C* **2016**, *120* (43), 24743−24753.
(35) Phan, A.; Cole, D. R.; Striolo, A. Preferential Adsorption from Liquid Water-Ethanol Mixtures in Alumina Pores. *Langmuir* **2014**, *30* (27), 8066−8077.
(36) Le, T.; Striolo, A.; Cole, D. R. CO2-C4H10 Mixtures Simulated in Silica Slit Pores: Relation between Structure and Dynamics. *J. Phys. Chem. C* **2015**, *119* (27), 15274−15284.
(37) Bui, T.; Phan, A.; Cole, D. R.; Striolo, A. Transport Mechanism of Guest Methane in Water-Filled Nanopores. *J. Phys. Chem. C* **2017**, *121* (29), 15675−15686.
(38) Gelb, L. D.; Gubbins, K. E.; Radhakrishnan, R.; Sliwinska-Bartkowiak, M. Phase separation in confined systems. *Rep. Prog. Phys.* **1999**, *62* (12), 1573−1659.
(39) Luzar, A.; Bratko, D. Gas solubility in hydrophobic confinement. *J. Phys. Chem. B* **2005**, *109* (47), 22545−22552.
(40) Bratko, D.; Luzar, A. Attractive surface force in the presence of dissolved gas: A molecular approach. *Langmuir* **2008**, *24* (4), 1247−1253.
(41) Pera-Titus, M.; El-Chahal, R.; Rakotovao, V.; Daniel, C.; Miachon, S.; Dalmon, J. A. Direct Volumetric Measurement of Gas Oversolubility in Nanoliquids: Beyond Henry's Law. *ChemPhysChem* **2009**, *10* (12), 2082−2089.
(42) Rakotovao, V.; Ammar, R.; Miachon, S.; Pera-Titus, M. Influence of the mesoconfining solid on gas oversolubility in nanoliquids. *Chem. Phys. Lett.* **2010**, *485* (4−6), 299−303.
(43) Hu, Y. F.; Huang, L. L.; Zhao, S. L.; Liu, H. L.; Gubbins, K. E. Effect of confinement in nano-porous materials on the solubility of a supercritical gas. *Mol. Phys.* **2016**, *114* (22), 3294−3306.
(44) Phan, A.; Cole, D. R.; Striolo, A. Factors governing the behaviour of aqueous methane in narrow pores. *Philos. Trans. R. Soc., A* **2016**, *374* (2060), 20150019.
(45) Phan, A.; Cole, D. R.; Weiss, R. G.; Dzubiella, J.; Striolo, A. Confined Water Determines Transport Properties of Guest Molecules in Narrow Pores. *ACS Nano* **2016**, *10* (8), 7646−7656.
(46) Moucka, F.; Svoboda, M.; Lisal, M. Modelling aqueous solubility of sodium chloride in clays at thermodynamic conditions of hydraulic fracturing by molecular simulations. *Phys. Chem. Chem. Phys.* **2017**, *19* (25), 16586−16599.
(47) Moucka, F.; Bratko, D.; Luzar, A. Electrolyte pore/solution partitioning by expanded grand canonical ensemble Monte Carlo simulation. *J. Chem. Phys.* **2015**, *142* (12), 124705.
(48) Bonthuis, D. J.; Gekle, S.; Netz, R. R. Dielectric Profile of Interfacial Water and its Effect on Double-Layer Capacitance. *Phys. Rev. Lett.* **2011**, DOI: 10.1103/PhysRevLett.107.166102.
(49) Bratko, D.; Daub, C. D.; Luzar, A. Water-mediated ordering of nanoparticles in an electric field. *Faraday Discuss.* **2009**, *141*, 55−66.
(50) Zhang, C.; Gygi, F.; Galli, G. Strongly Anisotropic Dielectric Relaxation of Water at the Nanoscale. *J. Phys. Chem. Lett.* **2013**, *4* (15), 2477−2481.
(51) Renou, R.; Szymczyk, A.; Ghoufi, A. Tunable dielectric constant of water at the nanoscale. *Phys. Rev. E* **2015**, DOI: 10.1103/PhysRevE.91.032411.
(52) Schlaich, A.; Knapp, E. W.; Netz, R. R. Water Dielectric Effects in Planar Confinement. *Phys. Rev. Lett.* **2016**, DOI: 10.1103/PhysRevLett.117.048001.
(53) Patankar, S.; Gautam, S.; Rother, G.; Podlesnyak, A.; Ehlers, G.; Liu, T. L.; Cole, D. R.; Tomasko, D. L. Role of Confinement on Adsorption and Dynamics of Ethane and an Ethane-CO2Mixture in Mesoporous CPG Silica. *J. Phys. Chem. C* **2016**, *120* (9), 4843−4853.
(54) Bazilevskaya, E.; Rother, G.; Mildner, D. F. R.; Pavich, M.; Cole, D.; Bhatt, M. P.; Jin, L. X.; Steefel, C. I.; Brantley, S. L. How Oxidation and Dissolution in Diabase and Granite Control Porosity during Weathering. *Soil Sci. Soc. Am. J.* **2015**, *79* (1), 55−73.
(55) Ma, L.; Fauchille, A.-L.; Dowey, P. J.; Figueroa Pilz, F.; Courtois, L.; Taylor, K. G.; Lee, P. D. *Correlative multi-scale imaging of shales: a*

DOI: 10.1021/acs.energyfuels.7b01023
Energy Fuels XXXX, XXX, XXX−XXX

review and future perspectives; Geological Society, London, Special Publications, 2017, p *454*.
(56) Ma, L.; Taylor, K. G.; Lee, P. D.; Dobson, K. J.; Dowey, P. J.; Courtois, L. Novel 3D centimetre-to nano-scale quantification of an organic-rich mudstone: The Carboniferous Bowland Shale, Northern England. *Mar. Pet. Geol.* **2016**, *72*, 193−205.
(57) Chen, C.; Hu, D. D.; Westacott, D.; Loveless, D. Nanometer-scale characterization of microscopic pores in shale kerogen by image analysis and pore-scale modeling. *Geochem., Geophys., Geosyst.* **2013**, *14* (10), 4066−4075.
(58) Goldstein, J. *Scanning Electron Microscopy and X-ray Microanalysis*, Third ed.; Springer: New York, 2003; p 695.
(59) Heath, J. E.; Dewers, T. A.; McPherson, B. J. O. L.; Petrusak, R.; Chidsey, T. C.; Rinehart, A. J.; Mozley, P. S. Pore networks in continental and marine mudstones: Characteristics and controls on sealing behavior. *Geosphere* **2011**, *7* (2), 429−454.
(60) Zhang, S.; Klimentidis, R. E.; Barthelemy, P. Porosity and permeability analysis on nanoscale FIB-SEM 3D imaging of shale rock. In *International Symposium of the Society of Core Analysts* Austin, Texas, Sep 18−21, 2011.
(61) Curtis, M. E.; Sondergeld, C. H.; Ambrose, R. J.; Rai, C. S. Microstructural investigation of gas shales in two and three dimensions using nanometer-scale resolution imaging. *AAPG Bull.* **2012**, *96* (4), 665−677.
(62) Landrot, G.; Ajo-Franklin, J. B.; Yang, L.; Cabrini, S.; Steefel, C. I. Measurement of accessible reactive surface area in a sandstone, with application to CO2 mineralization. *Chem. Geol.* **2012**, *318*, 113−125.
(63) Camp, W. K.; Diaz, E.; Wawak, B.; Geologists, A. A. P.; Petroleum, B.; Ingrain, I.; Laboratories, W.; Laboratories, C. *Electron Microscopy of Shale Hydrocarbon Reservoirs: AAPG Memoir 102*; American Association of Petroleum Geologists, 2013; p 260.
(64) Silin, D.; Kneafsey, T. Shale Gas: Nanometer-Scale Observations and Well Modelling. *J. Can. Petrol Technol.* **2012**, *51* (6), 464−475.
(65) Arthur, M. A.; Cole, D. R. Unconventional Hydrocarbon Resources: Prospects and Problems. *Elements* **2014**, *10* (4), 257−264.
(66) Heller, R.; Zoback, M. Adsorption of methane and carbon dioxide on gas shale and pure mineral samples. *Journal of Unconventional Oil and Gas Resources* **2014**, *8*, 14−24.
(67) Brennan, J. K.; Thomson, K. T.; Gubbins, K. E. Adsorption of water in activated carbons: Effects of pore blocking and connectivity. *Langmuir* **2002**, *18* (14), 5438−5447.
(68) Bhandari, A. R.; Flemings, P. B.; Polito, P. J.; Cronin, M. B.; Bryant, S. L. Anisotropy and Stress Dependence of Permeability in the Barnett Shale. *Transp. Porous Media* **2015**, *108* (2), 393−411.
(69) Ghanizadeh, A.; Gasparik, M.; Amann-Hildenbrand, A.; Gensterblum, Y.; Krooss, B. M. Experimental study of fluid transport processes in the matrix system of the European organic-rich shales: I. Scandinavian Alum Shale. *Mar. Pet. Geol.* **2014**, *51*, 79−99.
(70) Ghanizadeh, A.; Amann-Hildenbrand, A.; Gasparik, M.; Gensterblum, Y.; Krooss, B. M.; Littke, R. Experimental study of fluid transport processes in the matrix system of the European organic-rich shales: II. Posidonia Shale (Lower Toarcian, northern Germany). *Int. J. Coal Geol.* **2014**, *123*, 20−33.
(71) Heller, R.; Vermylen, J.; Zoback, M. Experimental investigation of matrix permeability of gas shales. *AAPG Bull.* **2014**, *98* (5), 975−995.
(72) Chalmers, G. R. L.; Ross, D. J. K.; Bustin, R. M. Geological controls on matrix permeability of Devonian Gas Shales in the Horn River and Liard basins, northeastern British Columbia, Canada. *Int. J. Coal Geol.* **2012**, *103*, 120−131.
(73) Bustin, R. M.; Bustin, A. M. M.; Cui, A.; Ross, D.; Pathi, V. M. Impact of Shale Properties on Pore Structure and Storage Characteristics. *SPE Shale Gas Prod. Conf.* **2008**, DOI: 10.2118/119892-MS.
(74) Tinni, A.; Fathi, E.; Agarwal, R.; Sondergeld, C. H.; Akkutlu, I. Y.; Rai, C. S. Shale Permeability Measurements on Plugs and Crushed Samples. *SPE Can. Unconventional Resources Conf.* **2012**, 1 DOI: 10.2118/162235-MS.
(75) Metwally, Y. M.; Sondergeld, C. H. Measuring low permeabilities of gas-sands and shales using a pressure transmission technique. *Int. J. Rock Mech Min* **2011**, *48* (7), 1135−1144.
(76) Pathi, V. S. M. Factors affecting the permeability of gas shales. *Master of Science Text*; University of British Columbia, 2008.
(77) Cygan, R. T.; Liang, J. J.; Kalinichev, A. G. Molecular models of hydroxide, oxyhydroxide, and clay phases and the development of a general force field. *J. Phys. Chem. B* **2004**, *108* (4), 1255−1266.
(78) Loganathan, N.; Yazaydin, A. O.; Bowers, G. M.; Kalinichev, A. G.; Kirkpatrick, R. J. Structure, Energetics, and Dynamics of Cs+ and H2O in Hectorite: Molecular Dynamics Simulations with an Unconstrained Substrate Surface. *J. Phys. Chem. C* **2016**, *120* (19), 10298−10310.
(79) Benjamin, I. Chemical reactions and solvation at liquid interfaces: A microscopic perspective. *Chem. Rev.* **1996**, *96* (4), 1449−1475.
(80) Greathouse, J. A.; Cygan, R. T. Water structure and aqueous uranyl(VI) adsorption equilibria onto external surfaces of beidellite, montmorillonite, and pyrophyllite: Results from molecular simulations. *Environ. Sci. Technol.* **2006**, *40* (12), 3865−3871.
(81) Hensen, E. J. M.; Smit, B. Why clays swell. *J. Phys. Chem. B* **2002**, *106* (49), 12664−12667.
(82) Holmboe, M.; Bourg, I. C. Molecular Dynamics Simulations of Water and Sodium Diffusion in Smectite Interlayer Nanopores as a Function of Pore Size and Temperature. *J. Phys. Chem. C* **2014**, *118* (2), 1001−1013.
(83) Marry, V.; Turq, P. Microscopic simulations of interlayer structure and dynamics in bihydrated heteroionic montmorillonites. *J. Phys. Chem. B* **2003**, *107* (8), 1832−1839.
(84) Newton, A. G.; Kwon, K. D.; Cheong, D. K. Edge Structure of Montmorillonite from Atomistic Simulations. *Minerals* **2016**, *6* (2), 25.
(85) Newton, A. G.; Sposito, G. Molecular Dynamics Simulations of Pyrophyllite Edge Surfaces: Structure, Surface Energies, and Solvent Accessibility. *Clays Clay Miner.* **2015**, *63* (3−4), 277−289.
(86) Tesson, S.; Salanne, M.; Rotenberg, B.; Tazi, S.; Marry, V. Classical Polarizable Force Field for Clays: Pyrophyllite and Talc. *J. Phys. Chem. C* **2016**, *120* (7), 3749−3758.
(87) Ungerer, P.; Collell, J.; Yiannourakou, M. Molecular Modeling of the Volumetric and Thermodynamic Properties of Kerogen: Influence of Organic Type and Maturity. *Energy Fuels* **2015**, *29* (1), 91−105.
(88) Kelemen, S. R.; Afeworki, M.; Gorbaty, M. L.; Sansone, M.; Kwiatek, P. J.; Walters, C. C.; Freund, H.; Siskin, M.; Bence, A. E.; Curry, D. J.; Solum, M.; Pugmire, R. J.; Vandenbroucke, M.; Leblond, M.; Behar, F. Direct characterization of kerogen by x-ray and solid-state 13C nuclear magnetic resonance methods. *Energy Fuels* **2007**, *21* (3), 1548−1561.
(89) Orendt, A. M.; Pimienta, I. S. O.; Badu, S. R.; Solum, M. S.; Pugmire, R. J.; Facelli, J. C.; Locke, D. R.; Chapman, K. W.; Chupas, P. J.; Winans, R. E. Three-Dimensional Structure of the Siskin Green River Oil Shale Kerogen Model: A Comparison between Calculated and Observed Properties. *Energy Fuels* **2013**, *27* (2), 702−710.
(90) Palmer, J. C.; Gubbins, K. E. Atomistic models for disordered nanoporous carbons using reactive force fields. *Microporous Mesoporous Mater.* **2012**, *154*, 24−37.
(91) Palmer, J. C.; Llobet, A.; Yeon, S. H.; Fischer, J. E.; Shi, Y.; Gogotsi, Y.; Gubbins, K. E. Modeling the structural evolution of carbide-derived carbons using quenched molecular dynamics. *Carbon* **2010**, *48* (4), 1116−1123.
(92) Palmer, J. C.; Brennan, J. K.; Hurley, M. M.; Balboa, A.; Gubbins, K. E. Detailed structural models for activated carbons from molecular simulation. *Carbon* **2009**, *47* (12), 2904−2913.
(93) Vasileiadis, M.; Peristeras, L. D.; Papavasileiou, K. D.; Economou, I. G. Modeling of Bulk Kerogen Porosity: Methods for Control and Characterization. *Energy Fuels* **2017**, *31* (6), 6004−6018.
(94) Ross, H. E.; Hagin, P.; Zoback, M. D. CO2 storage and enhanced coalbed methane recovery: Reservoir characterization and fluid flow simulations of the Big George coal, Powder River Basin, Wyoming, USA. *Int. J. Greenhouse Gas Control* **2009**, *3* (6), 773−786.

DOI: 10.1021/acs.energyfuels.7b01023
Energy Fuels XXXX, XXX, XXX−XXX

(95) Zachara, J.; Brantley, S.; Chorover, J.; Ewing, R.; Kerisit, S.; Liu, C. X.; Perfect, E.; Rother, G.; Stack, A. G. Internal Domains of Natural Porous Media Revealed: Critical Locations for Transport, Storage, and Chemical Reaction. *Environ. Sci. Technol.* **2016**, *50* (6), 2811−2829.
(96) Balhoff, M. T.; Thompson, K. E.; Hjortso, M. Coupling pore-scale networks to continuum-scale models of porous media. *Comput. Geosci.* **2007**, *33* (3), 393−410.
(97) Chen, L.; Zhang, L.; Kang, Q. J.; Viswanathan, H. S.; Yao, J.; Tao, W. Q. Nanoscale simulation of shale transport properties using the lattice Boltzmann method: permeability and diffusivity. *Sci. Rep.* **2015**, DOI: 10.1038/srep08089.
(98) Succi, S. Mesoscopic Modeling of Slip Motion at Fluid-Solid Interfaces with Heterogeneous Catalysis. *Phys. Rev. Lett.* **2002**, *89* (6), 064502.
(99) Bonilla, M. R.; Valiullin, R.; Karger, J.; Bhatia, S. K. Understanding Adsorption and Transport of Light Gases in Hierarchical Materials Using Molecular Simulation and Effective Medium Theory. *J. Phys. Chem. C* **2014**, *118* (26), 14355−14370.
(100) Lock, P. A.; Jing, X. D.; Zimmerman, R. W.; Schlueter, E. M. Predicting the permeability of sandstone from image analysis of pore structure. *J. Appl. Phys.* **2002**, *92* (10), 6311−6319.
(101) Lock, P. A.; Jing, X. D.; Zimmerman, R. W. Comparison of methods for upscaling permeability from the pore scale to the core scale. *J. Hydraul Res.* **2004**, *42*, 3−8.
(102) Bernasconi, J. Conduction in Anisotropic Disordered Systems - Effective-Medium Theory. *Phys. Rev. B* **1974**, *9* (10), 4575−4579.
(103) Liu, X.; Newsome, D.; Coppens, M. O. Dynamic Monte Carlo simulations of binary self-diffusion in ZSM-5. *Microporous Mesoporous Mater.* **2009**, *125* (1−2), 149−159.
(104) Galarneau, A.; Guenneau, F.; Gedeon, A.; Mereib, D.; Rodriguez, J.; Fajula, F.; Coasne, B. Probing Interconnectivity in Hierarchical Microporous/Mesoporous Materials Using Adsorption and Nuclear Magnetic Resonance Diffusion. *J. Phys. Chem. C* **2016**, *120* (3), 1562−1569.
(105) Flamm, M. H.; Diamond, S. L.; Sinno, T. Lattice kinetic Monte Carlo simulations of convective-diffusive systems. *J. Chem. Phys.* **2009**, *130* (9), 094904.
(106) Stamatakis, M. Kinetic modelling of heterogeneous catalytic systems. *J. Phys.: Condens. Matter* **2015**, *27* (1), 013001.
(107) Battaile, C. C.; Srolovitz, D. J. Kinetic Monte Carlo simulation of chemical vapor deposition. *Annu. Rev. Mater. Res.* **2002**, *32*, 297−319.
(108) Yang, X.; Hassanein, A. Kinetic Monte Carlo simulation of hydrogen diffusion on tungsten reconstructed (001) surface. *Fusion Eng. Des.* **2014**, *89* (11), 2545−2549.
(109) Dai, J.; Seider, W. D.; Sinno, T. Lattice kinetic Monte Carlo simulations of defect evolution in crystals at elevated temperature. *Mol. Simul.* **2006**, *32* (3−4), 305−314.
(110) Voter, A. F. Introduction to the Kinetic Monte Carlo Method. *Nato Sci. Ser. Ii-Math* **2007**, *235*, 1−23.
(111) Kratzer, P. *Monte Carlo and Kinetic Monte Carlo Methods A Tutorial*; 2009; Vol. *42*.
(112) Newsome, D.; Coppens, M. O. Molecular dynamics as a tool to study heterogeneity in zeolites - Effect of Na+ cations on diffusion of CO2 and N-2 in Na-ZSM-5. *Chem. Eng. Sci.* **2015**, *121*, 300−312.
(113) Apostolopoulou, M.; Stamatakis, M.; Striolo, A. A Kinetic Monte Carlo Framework for Multi-Phase Fluid Transport in Heterogeneous Pore Networks. *J. Chem. Phys.* **2017**, in press.
(114) Kärger, J.; Ruthven, D. M.; Theodorou, D. N. *Diffusion in Nanoporous Materials*; Wiley, 2012.
(115) Brandani, S.; Hufton, J.; Ruthven, D. Self-Diffusion of Propane and Propylene in 5a and 13x Zeolite Crystals Studied by the Tracer Zlc Method. *Zeolites* **1995**, *15* (7), 624−631.
(116) Ruthven, D. M. *Principles of Adsorption and Adsorption Processes*; Wiley: New York, 1984.
(117) Karger, J.; Pfeifer, H. N.m.r Self-Diffusion Studies in Zeolite Science and Technology. *Zeolites* **1987**, *7* (2), 90−107.
(118) Gupta, A.; Snurr, R. Q. A study of pore blockage in silicalite zeolite using free energy perturbation calculations. *J. Phys. Chem. B* **2005**, *109* (5), 1822−1833.
(119) Falk, K.; Coasne, B.; Pellenq, R.; Ulm, F. J.; Bocquet, L. Subcontinuum mass transport of condensed hydrocarbons in nanoporous media. *Nat. Commun.* **2015**, *6*, 6949.
(120) Obliger, A.; Pellenq, R.; Ulm, F. J.; Coasne, B. Free Volume Theory of Hydrocarbon Mixture Transport in Nanoporous Materials. *J. Phys. Chem. Lett.* **2016**, *7* (19), 3712−3717.
(121) Ho, T. A.; Criscenti, L. J.; Wang, Y. F. Nanostructural control of methane release in kerogen and its implications to wellbore production decline. *Sci. Rep.* **2016**, DOI: 10.1038/srep28053.
(122) Lee, T.; Bocquet, L.; Coasne, B. Activated desorption at heterogeneous interfaces and long-time kinetics of hydrocarbon recovery from nanoporous media. *Nat. Commun.* **2016**, *7*, 11890.
(123) Ho, T. A.; Striolo, A. Water and methane in shale rocks: Flow pattern effects on fluid transport and pore structure. *AIChE J.* **2015**, *61* (9), 2993−2999.
(124) Ellis, B. R.; Peters, C. A. 3D Mapping of calcite and a demonstration of its relevance to permeability evolution in reactive fractures. *Adv. Water Resour.* **2016**, *95*, 246−253.
(125) Ercius, P.; Alaidi, O.; Rames, M. J.; Ren, G. Electron Tomography: A Three-Dimensional Analytic Tool for Hard and Soft Materials Research. *Adv. Mater.* **2015**, *27* (38), 5638−5663.
(126) Midgley, P. A.; Weyland, M. 3D electron microscopy in the physical sciences: the development of Z-contrast and EFTEM tomography. *Ultramicroscopy* **2003**, *96* (3−4), 413−431.
(127) Li, H. Y.; Xin, H. L.; Muller, D. A.; Estroff, L. A. Visualizing the 3D Internal Structure of Calcite Single Crystals Grown in Agarose Hydrogels. *Science* **2009**, *326* (5957), 1244−1247.
(128) McNally, E.; Nan, F. H.; Botton, G. A.; Schwarcz, H. P. Scanning transmission electron microscopic tomography of cortical bone using Z-contrast imaging. *Micron* **2013**, *49*, 46−53.
(129) Wills, A. W.; Michalak, D. J.; Ercius, P.; Rosenberg, E. R.; Perciano, T.; Ushizima, D.; Runser, R.; Helms, B. A. Block Copolymer Packing Limits and Interfacial Reconfigurability in the Assembly of Periodic Mesoporous Organosilicas. *Adv. Funct. Mater.* **2015**, *25* (26), 4120−4128.
(130) Ercius, P.; Xin, H. L. L.; Muller, D. A. Measurements of Porous Networks in Low-k Dielectric by Three-dimensional Electron Tomography. *Microsc. Microanal.* **2009**, *15*, 1240−1241.
(131) Taylor, R.; Sakdinawat, A.; Chae, S. R.; Wenk, H. R.; Levitz, P.; Sougrat, R.; Monteiro, P. J. M. Developments in TEM Nano-tomography of Calcium Silicate Hydrate. *J. Am. Ceram. Soc.* **2015**, *98* (7), 2307−2312.
(132) King, H. E., Jr.; Eberle, A. P. R.; Walters, C. C.; Kliewer, C. E.; Ertas, D. Pore architecture and connectivity in gas shale. *Energy Fuels* **2015**, *29* (3), 1375−1390.
(133) Lash, G. G.; Engelder, T. An analysis of horizontal microcracking during catagenesis: Example from the Catskill delta complex. *AAPG Bull.* **2005**, *89* (11), 1433−1449.
(134) Fauchille, A. L.; Ma, L.; Rutter, E.; Chandler, M.; Lee, P. D.; Taylor, K. G. An enhanced understanding of the Basinal Bowland shale in Lancashire (UK), through microtextural and mineralogical observations. *Mar. Pet. Geol.* **2017**, *86*, 1374.
(135) Figueroa Pilz, F.; Dowey, P. J.; Fauchille, A. L.; Courtois, L.; Bay, B.; Ma, L.; Taylor, K. G.; Mecklenburgh, J.; Lee, P. D. Synchrotron tomographic quantification of strain and fracture during simulated thermal maturation of an organic-rich shale, UK Kimmeridge Clay. *J. Geophys Res-Sol Ea* **2017**, *122* (4), 2553−2564.
(136) Fauchille, A. L. A. P.; Eijnden, v. d.; Ma, L.; Chandler, M.; Madi, K.; Taylor, K. G.; Lee, P. D.; Rutter, E. Variability of the spatial distribution of mineral phases in the Lower Bowland Shale from the μm to the mm scale: quantitative characterization and modelling, in preparation.
(137) ROXOL-the fracture network evolution simulator. http://www.roxol.de/.
(138) Nexus Suite Reservoir Simulation. https://www.landmark.solutions/Nexus-Reservoir-Simulation.

DOI: 10.1021/acs.energyfuels.7b01023
Energy Fuels XXXX, XXX, XXX−XXX